Original Paper

Landslides (2025) 22:1825–1840
DOI 10.1007/s10346-025-02456-4
Received: 27 March 2024
Accepted: 29 December 2024
Published online: 6 February 2025


Xi'an Wang · Jiangang Chen · Xiaoqing Chen · Huayong Chen · Wanyu Zhao · Xiangning Li · Wenjing Xu

# Regulating effect of wooded channels on debris flows

**Abstract** The channel forest is believed to possess the capability to regulate debris flow; however, its sediment trapping effect remains unclear. This study investigates the influence of tree trunk volume fraction (the proportion of trunk cross-sectional area to the woodland area and ranging from $0.9\times10^{-3}$ to $88.6\times10^{-3}$) on the deposition patterns and impact force of debris flow through a series of physical experiments. Upon entering the wooded channel, the velocity of the debris flow declined while the flow depth raised, eventually reaching a state of equilibrium in the new resistance environment. Simultaneously, a significant volume of sediment was trapped within the wooded channel. The deposition height decreased gradually from upstream to downstream, leading to an increase in bed slope within the forested area. The peak impact force attenuation rate ranged from 15.8 to 79.0%, while the sediment retention rate varied from 3.0 to 31.7%. Notably, peak impact force attenuation rate showed the strongest correlation with the relative opening, whereas the sediment retention rate exhibited the strongest relationship with the initial resistance energy slope of forest. It was observed that viscous debris flows exhibited a slightly lower peak impact force attenuation rate than diluted debris flows, whereas the opposite was true for the sediment retention rate. The bed slope increment caused by sediment deposition in wooded channel ranged from 0.002 to 0.089 and demonstrated a proportional relationship with the initial resistance energy slope of woods. Specifically, for viscous debris flows, the proportional coefficient was 2.3%, and for diluted debris flows, it was 3.4%. This study also introduces novel calculation methods for calculating the deposition slope and estimating potential sediment retained volume in wooded channels.

**Keywords** Debris flow · Wooded channels · Sediment trapping · Deposition slope · Impact force

## Notations

| | |
|---|---|
| $A_F$ | The attenuation rate of peak impact force |
| $A_S$ | The sediment retention rate |
| $B$ | The channel width of channel bed |
| $C_d$ | The woods drag coefficient |
| $C_f$ | The bed drag coefficient |
| $C_v$ | The sediment concentration of debris flow |
| $d$ | The tree trunk diameter |
| $d_{max}$ | The maximum particle size in a debris flow |
| $E(y)$ | The expectation of the deposition position |
| $F_o$ | The peak impact force on trunk located at array IV before the installation of model woods |
| $F_1$ | The peak impact force on trunk located at array IV after the installation of model woods |
| $Fr$ | The Froude number |
| $g$ | The gravitational acceleration |
| $h$ | The depth of debris flow |
| $h_o$ | The initial depth of debris flow |
| $H_{dep}$ | The sedimentation height |
| $H_{max}$ | The maximum deposition height |
| $k$ | The proportional coefficient between ΔSbed and ΔSe |
| $l$ | The tree spacing |
| $L$ | The distance between the measured point and the downstream edge of wooded channel |
| $L_{dep,max}$ | The distance between the location of maximum deposition height and the downstream edge of wooded channel |
| $L_{woods}$ | The horizontal length of woods |
| $m_o$ | The total mass of sediment in a debris flow surge |
| $m_1$ | The mass of trapped sediment |
| $N$ | The stand density of woods |
| $R_o$ | The relative opening, used to quantify the size of the tree spacing relative to the maximum particle size in a debris flow |
| $S_{bed}$ | The slope of channel bed |
| $S_{dep}$ | The deposition slope in wooded channel |
| $S_e$ | The energy slope of debris flow |
| $S_{init}$ | The initial slope of channel bed |
| $v$ | The velocity of debris flow |
| $v_o$ | The initial velocity of debris flow |
| $V_{dep}$ | The volume of trapped sediment |
| $y$ | The longitudinal section coordinates taking the downstream edge of the woods model as the coordinate origin and taking Lwoods as the unit length and the upstream horizontal direction to be positive direction |
| $Z$ | The collection of regulation indicators (AF, AS, ΔSbed) |
| $\Delta S_e$ | The resistance energy slope of woods |
| $\Delta S_{bed}$ | The bed slope increment caused by deposition in wooded channel |
| $\sigma(y)$ | The variance of the deposition position |
| $\pi$ | The pi |
| $\rho$ | The density of debris flow |
| $\phi$ | The tree trunks volume fraction |

## Introduction

Forests on both channels and slopes play a vital role in mitigating debris flows (Cui and Lin 2013; Stokes et al. 2014). The canopy and root systems in slope vegetation effectively reduce debris recharge

into channels, thus inhibiting debris flow occurrences. Several models have been developed to simulate and evaluate this process (Bathurst et al. 2010; Kim et al. 2013; Schwarz et al. 2013, 2015; Ng et al. 2016). Furthermore, a range of slope ecological engineering measures has been devised to enhance soil and water conservation and intercept sediment. These measures include contour tillage, the transformation of sloping fields into terraces, contour hedgerows, and the planting of trees and grass (Cui and Lin 2013; He et al. 2017). In contrast to the flow interception and sediment reduction effects of forests on slopes (Imaizumi et al. 2008; Liu et al. 2023), the impact of forests within channels remains relatively unexplored. Some bioengineering measures, such as botanical check dams, wooden sills, and vegetation filter zones with wooden sills, were tentatively employed in channels to enhance ecological restoration and strengthen disaster mitigation efforts (Rey and Burylo 2014; Rey et al. 2019). Some debris flow channels contain forests (Zhou et al. 2023; Cui et al. 2024). The diameter at breast height of these trees is greater than 10 cm, and their height exceeds 8 m (see Table 1). The tree height is significantly greater than the flow depth of the debris flows. Existing field observations indicate that the flow depth of debris flows does not exceed 6 m, and in most cases, it is less than 4 m (Phillips and Davies 1991; Du et al. 2023). Forests require sufficient time to mature and exert their regulatory effects on debris flows; therefore, they primarily influence low-frequency debris flows rather than high-frequency ones. Field cases have confirmed that forests can regulate the energy of debris flows and trap sediment (Ishikawa et al. 2003; Malik et al. 2013; Michelini et al. 2017; Cui et al. 2023a). However, comprehensive physical model tests to fully understand the regulatory influence of wooded channels on debris flows are lacking.

Physical model tests evaluating the impact of baffle arrays and slit dams on debris flow regulation have been extensively studied (Ng et al. 2014; Piton and Recking 2016; Silva et al. 2016; Goodwin and Choi 2020; Wang et al. 2020). The spacing and distribution of tree trunks or baffles significantly influence the development of bow shock waves and the movement of debris flows (Liang et al. 2023). In addition, large particles can also form an arch structure, obstructing these openings and influencing the passage of subsequent debris flows (Shima et al. 2016; Zhang et al. 2021). Hence, the relative opening degree, defined as the ratio of gap width to the maximum particle diameter, significantly influences debris flow regulation (Zhou et al. 2019a) and serves as a crucial parameter in engineering design (Piton and Recking 2016; Sun et al. 2018; Piton et al. 2022). A comparable process may occur in forest environments, making the consideration of relative openings pertinent in this study. However, the stand density of baffle arrays in channel far exceeds that of natural forests (Table 2), and the number of rows (the distribution area) of baffle arrays is significantly smaller compared to channel forests (Ishihara et al. 2011; Ng et al. 2014; Põldveer et al. 2020; Kim et al. 2023; Wu et al. 2023). For baffle arrays, low array density is considered to have limited regulatory effects (Goodwin et al. 2021). In contrast, the trees in debris flow channels often have more rows and occupy part or all of the channel, suggesting that even at low stand densities, forests may still possess considerable regulatory capacity.

The impact of river vegetation on reducing flow velocity and retaining sediment has been extensively documented (Nepf 2012; Vargas-Luna et al. 2018; Lightbody et al. 2019; Li et al. 2020; Khoshkonesh et al. 2022). This phenomenon is primarily governed by factors such as stem volume fraction (Shan et al. 2020; Liu et al. 2021; Wang et al. 2023). Vegetation resistance plays a crucial role in influencing flow velocity and turbulence (Tanino and Nepf 2008; Tinoco and Coco 2016; Yang and Nepf 2018; Shan et al. 2020). Flow velocity serves as a vital indicator for debris flow mitigation (Chen et al. 2015; Piton and Recking 2016), while turbulent kinetic energy is believed to significantly impact sediment transport and deposition processes (Yang and Nepf 2019; Liu et al. 2022). Debris flows typically surge down steep slope channels, exhibiting material composition, flow processes, and movement characteristics that differ from river flows (Zanuttigh and Lamberti 2007; Kean et al. 2013; Borga et al. 2014; Pudasaini and Mergili 2019; Guo et al. 2020; Huebl and Kaitna 2021). Due to limited research and measurement methods regarding debris flow turbulence (Enos 1977; Jan and Shen 1997; Trujillo-Vela et al. 2022), forest resistance emerges as a crucial parameter in studies on the regulation of debris flow by forests.

In this study, we aim to investigate the influence of tree trunk volume fraction, relative opening degree, and forest resistance characteristics (quantified by the initial resistance energy slope of the woods) on debris flow impact force attenuation and sediment retention. Through physical model experiments, our research takes a preliminary step toward understanding the mitigation potential of wooded channels against debris flows. Additionally, these findings provide valuable insights for the application of nature-based solutions in debris flow mitigation strategies.

## Material and methods

### Experimental setup

The experiments were conducted at the Dongchuan Debris Flow Observation and Research Station, Chinese Academy of Sciences, Yunnan, China. The test device consisted a hopper, a flume, and model woods (Fig. 1).

**Table 1** Diameter at breast height (DBH) and height of trees in debris flow channels

| Location | Dominant species | DBH (m) | Tree height* (m) | References |
|---|---|---|---|---|
| Southern Fukushima and Hiroshima, Japan | *Cryptomeria japonica*, *Pinus densiflora* | 0.10–0.48 | 8.0–35.3 | Ishikawa et al. 2003 |
| Belluno and Bolzano, Italy | *Picea abies*, *Pinus sylvestris* | 0.10–0.92 | 8.0–52 | Michelini et al. 2017 |
| Jiuzhaigou Valley, China | *Pinus tabuliformis* | 0.12–0.58 | 9.6–40.4 | Cui et al. 2024 |

Note: *The heights are the estimation value based on DBH (Bi et al. 2012)

**Table 2** Comparison of geometric parameters of forests and baffles (including field and experimental data)

| Subjects | Material type | Cross-section shape | Diameter or edge length (mm) | Spacing (mm) | Trunk volume fraction* ($\times 10^{-3}$) | References |
|---|---|---|---|---|---|---|
| Field forests | Wood | Circle | 10–404 | 1387–18594 | 0.02–13.9 | Wu et al. (2023) |
| Field forests | Wood | Circle | 112–325 | 20230–7098 | 1.5–7.0 | Põldveer et al. (2020) |
| Field forests | Wood | Circle | 99–491 | 1634–9050 | 0.9–12.5 | Ishihara et al. (2011) |
| Laboratory baffles in channel | Stainless steel | Circle | 30, 219 | 75 × 200, 281 × 1500 | 47.1–89.4 | Kim et al. (2023) |
| Laboratory baffles in channel | Steel | Triangle, rectangle | 50 | 50 × (150, 300) | 36.1–166.7 | Wang et al. (2017) |
| Laboratory baffles in channel | Aluminum | Rectangle | 20 | 67 × (70–270) | 22.1–85.3 | Choi et al. (2015c) |
| Laboratory baffles in channel | Aluminum | Rectangle | 20 × 20, 20 × 37 | (66, 100) × (70, 120) | 33.3–105.7 | Ng et al. (2015) |
| Laboratory baffles in board | Iron | Circle, rectangle, arc-shape | 50 | 50 × (100–160) | 59.3–250 | Wang et al. (2020) |
| Laboratory forests in board | Aluminum | Circle | 20 | 175 × 152, 350 × 303 | 2.9–11.8 | Liang et al. (2023) |
| Laboratory forests in board | Steel | Circle | 6 | 100 × 87 | 3.3 | Bettella et al. (2018) |

Note: *To quantify the proportion of trunks (baffles) cross-sectional area to the woodlands area

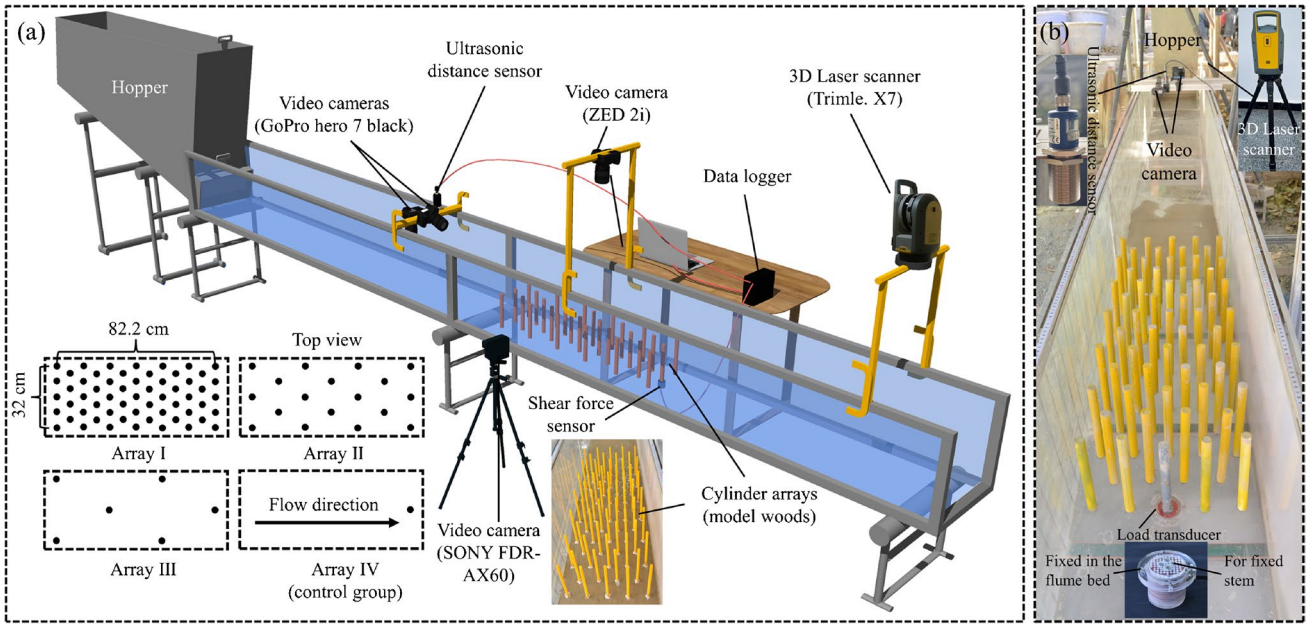


**Fig. 1** Experimental setup. **a** Schematic diagram; **b** Photograph

The hopper was used to temporarily store the debris flow material and guide debris flow material into the flume. The flume was constructed with acrylic material and had a rectangular cross-section, measuring 5.0 m in length, 0.4 m in width, and 0.4 m in height. It was divided into three sections: the incoming flow section, the model woods section, and the tailing section. In

the incoming flow section spanned approximately 3 m, which was used to stabilize the flow pattern of the debris flow. The model woods section is approximately 1 m; acrylic cylinders with a height of about 20 cm and a diameter of 1, 2, 3, 4, and 5 cm were used to simulate tree trunks; the acrylic cylinders were arranged according to four arrays (arrays I–IV) to simulate the forest with different stand density. Field observation data confirm that the flow depth of debris flows is significantly less than the height of the channel forest (Table 1; Phillips and Davies 1991; Du et al. 2023). Therefore, in our experiments, we controlled the flow depth of the debris flows to ensure that the tree trunk models were not submerged. The height of model trunks is approximately twice the peak flow depth in this study because the studies by Choi et al. (2014) and Ng et al. (2015) found that the increase in flow depth caused by baffles was mostly less than twice the original flow depth. Our physical models are primarily used to simulate evenly distributed cultivated forests. The tailing section, guiding the debris flow to the tailings collection vessel, is also about 1 m in length. The slope of the flume bed ($S_{init}$) was set at 0.15, which falls within the reasonable range (Rickenmann 1999).

### Experimental arrangement and measured variables

Table 3 presents the experimental arrangement and test conditions. During the tests, the morphological characteristics of channel before and after the debris flow surge were recorded by a 3D laser scanner (Trimble. X7, 6.40 ± 0.07 pts/cm²) (Fig. 1), and the collected point cloud data was utilized to generate digital elevation models (DEMs). The volume and distribution of trapped sediments were then determined by comparing repeat DEMs (DEMs collected at the same location over different time periods) (Brasington et al. 2012; Yang et al. 2021a, b). The regulating process was recorded by a video camera positioned at the top of the flume (ZED 2i, 1920 × 1080 pixels, 30 fps) (Fig. 1), and a video camera positioned at the upstream of model woods (GoPro Hero7 Black, 1920 × 1080 pixels, 120 fps) (Fig. 1), as well as another video camera placed on the right side of the flume (SONY FDR-AX60, 4096 × 2160 pixels, 50 fps).

The flow process and depth of the debris flow at approximately 1 m upstream of the model woods were recorded using a video camera (GoPro Hero7 Black, 1920 × 1080 pixels, 120 fps) and an ultrasonic distance sensor (CONTROLWAY mic + , accuracy 0.1 mm, sampling frequency 100 Hz) positioned on the top of the flume, respectively (Fig. 1). The assessment of flow velocity is based on flow depth, debris flow volume, and the assumption of a fixed Manning's roughness coefficient (see Appendix for details). This method offers a rough overall evaluation of the flow velocity. For precise measurements of flow velocity, the solution provided by Choi and Liang (2024) can be referenced. The impact force of the debris flow on the model trunk at the downstream side of model woods (array IV in Fig. 1) was recorded by a shear force sensor (JUL-3D46, capacity 10 kg, accuracy 0.01 N, sampling frequency 100 Hz) mounted on the base plate, and the measured model trunk is fixed to the probe of the shear force sensor. The entire impact force measurement system essentially meets the design standards proposed by Goodwin and Choi (2021).

**Table 3** Experimental arrangement and test conditions

| Case | $C_v$ | Model woods | | | | |
|---|---|---|---|---|---|---|
| | | $d$ (cm) | $l$ (cm) | $N$ (m$^{-2}$) | $\phi$ (×10$^{-3}$) | Array |
| D1_L8_C0.5*, D1_L8_C0.3* | 0.5, 0.3 | 1 | 8 | 180.4 | 14.2 | I |
| D1_L16_C0.5*, D1_L16_C0.3* | | 1 | 16 | 45.1 | 3.5 | II |
| D1_L32_C0.5*, D1_L32_C0.3* | | 1 | 32 | 11.3 | 0.9 | III |
| D1_L-_C0.5*†, D1_L-_C0.3*† | | 1 | - | - | - | IV |
| D2_L8_C0.5*, D2_L8_C0.3* | | 2 | 8 | 180.4 | 56.7 | I |
| D2_L16_C0.5*, D2_L16_C0.3 20* | | 2 | 16 | 45.1 | 14.2 | II |
| D2_L32_C0.5*, D2_L32_C0.3* | | 2 | 32 | 11.3 | 3.5 | III |
| D2_L-_C0.5*†, D2_ L-_C0.3*† | | 2 | - | - | - | IV |
| D3_L16_C0.5, D3_L16_C0.3 | | 3 | 16 | 45.1 | 31.9 | II |
| D3_L32_C0.5, D3_L32_C0.3 | | 3 | 32 | 11.3 | 8.0 | III |
| D4_L16_C0.5, D4_L16_C0.3 | | 4 | 16 | 45.1 | 56.7 | II |
| D4_L32_C0.5, D4_L32_C0.3 | | 4 | 32 | 11.3 | 14.2 | III |
| D5_L16_C0.5, D5_L16_C0.3 | | 5 | 16 | 45.1 | 88.6 | II |
| D5_L32_C0.5, D5_L32_C0.3 | | 5 | 32 | 11.3 | 22.1 | III |

Note: *For model woods with trunk diameters of 1 and 2 cm, we tested the impact force at the location of array IV; †we consider these experiments as blank control groups because only one trunk model used to measure impact force is installed in the flume

The main parameters used in this article are defined and calculated as follows:

(1) The tree trunk volume fraction

The tree trunk volume fraction ($\phi$), also known as solid volume fraction (Tanino and Nepf 2008; Liu et al. 2021), is used to quantify the proportion of trunk cross-sectional area to the woodland area:

$$\phi = N\pi d^2/4 \tag{1}$$

where $N$ is the stand density ($m^{-2}$), $\pi$ is the pi (-), and $d$ is the tree trunk diameter (m). The $\phi$ of field forests mainly ranges between $0.02\times10^{-3}$ and $14\times10^{-3}$ (Ishihara et al. 2011; Põldveer et al. 2020; Wu et al. 2023). Except for four blank control groups (D1,2_L-), 14 cases in this study (D1_AL8, D1,2_L16, D1,2,3,4_L32) are consistent with field conditions ($0.9\times10^{-3}$–$14.2\times10^{-3}$). Additionally, 10 cases (D2_L8, D3,4,5_L16, D5_L32) exhibit overly dense stems ($22.1\times10^{-3}$–$56.7\times10^{-3}$), which can be used to discuss the regulation effects of artificially dense forests or cylindrical baffles on debris flows.

(2) The relative opening

The relative opening ($R_o$), a parameter usually used in the study of baffle array and slit dam (Ng et al. 2014; Piton and Recking 2016; Goodwin and Choi 2020; Wang et al. 2020), is used to quantify the size of the tree spacing relative to the maximum particle size in a debris flow:

$$R_o = (l-d)/d_{max} \tag{2}$$

where $l$ is the tree spacing (m), $d$ is the tree trunk diameter (m), and $d_{max}$ is the maximum particle size in a debris flow (m), $d_{max}=20$ mm. $R_o$ ranges from 3.0 to 15.5 in this study.

(3) The initial resistance energy slope of woods

The initial resistance energy slope of woods ($\Delta S_e$) is used to quantify the ratio of wood resistance and gravity to debris flow when it just enters the woods. It also has the physical meaning of energy slope (Liu et al. 2021):

$$\Delta S_e = \frac{0.5C_d\rho v_0^2 h_0 dN}{\rho g h_0} = \frac{1}{2g}C_d\left(\frac{4\phi}{\pi d}\right)v_0^2 \tag{3}$$

$$S_e = \left[\frac{C_f}{gh} + \frac{1}{2g}C_d\left(\frac{4\phi}{\pi d}\right)\right]v^2 \tag{4}$$

where $C_d$ is the woods drag coefficient (-), we assumed $C_d=1$ in the study (Ishikawa et al. 2003). ρ is the density of debris flow ($kg/m^3$), $v_0$ is the initial velocity of debris flow (m/s), $h_0$ is the initial depth of debris flow (m), $d$ is the tree trunk diameter (m), $N$ is the number of trunks per square meter ($m^{-2}$), ϕ is the tree trunks volume fraction, $S_e$ is the energy slope of debris flow (-), $C_f$ is the bed drag coefficient (-), $v$ is the velocity of debris flow (m/s), and $h$ is the depth of debris flow (m).

(4) The attenuation rate of peak impact force ($A_F$), which characterizes the influence of channel woods as a whole on the debris flow impact force at its downstream end:

$$A_F = 1 - F_1/F_0 \tag{5}$$

where $F_0$ and $F_1$ are the peak impact force on trunk located at array IV before and after the installation of model woods, respectively ($N$). Because the variation in debris flow impact force can comprehensively reflect changes in flow depth, flow velocity, and material composition of debris flow (Kwan et al. 2024), $A_F$ effectively represents the overall regulation effect of channel forests on debris flows.

(5) The sediment retention rate ($A_S$) is one of the most widely used indicators to evaluate the effect of regulating debris flow (Sun et al. 2018; Li et al. 2019), which is often used to characterize the ratio of sediment trapped by engineering measures to total sediment in debris flow:

$$A_S = m_1/m_0 \tag{6}$$

where $m_0$ is the total mass of sediment in a debris flow surge(kg), and $m_1$ is the mass of trapped sediment (kg).

(6) The bed slope increment ($\Delta S_{bed}$) caused by deposition in wooded channel:

$$\Delta S_{bed} = S_{dep} - S_{init} = H_{max}/L_{dep,\,max} \tag{7}$$

where $S_{init}$ and $S_{dep}$ are the initial slope and deposition slope in wooded channel, respectively (-), $H_{max}$ is the maximum deposition height (m), and $L_{dep,\,max}$ is the distance between the location of maximum deposition height and the downstream edge of wooded channel (m).

(7) The longitudinal section coordinates ($y$):

$$y = L/L_{woods} \tag{8}$$

where $y$ represents the longitudinal section coordinates taking the downstream edge of the woods model as the coordinate origin and taking $L_{woods}$ as the unit length and the upstream horizontal direction to be positive direction, where $L$ is the distance between the measured point and the downstream edge of wooded channel (m); $L_{woods}$ is the horizontal length of woods (m).

## Materials and applicability

The granular material used in the tests was obtained from the debris flow deposition fan of Jiangjia Gully. Granular material with diameters larger than 20 mm was removed (Cui et al. 2015; Li et al. 2019). The particle size in debris flows significantly impacts jamming and deposition (Piton and Recking 2016; Gong et al. 2023) as well as impact force (Ng et al. 2021). In the experiments, efforts were made to control the composition and movement processes of the debris flows to minimize the influence of their inherent differences on the results. Figure 2 shows the particle size distribution of the granular material in the debris flow. The measured particle density ($\rho_s$) was 2680 $kg/m^3$. Some dimensionless parameters were controlled in the study, as the experimental design was based on general conditions of field cases. The sediment concentration ($C_v$) values of the debris flow were 0.5 and 0.3. When $C_v=0.5$, the flow is classified as a debris flow or viscous debris flow. When $C_v=0.3$, the flow is referred to as a debris flood or diluted debris flow (Iverson 1997; Kang et al. 2004; Church and Jakob 2020). For the convenience of expression, this paper uses viscous debris flow and diluted debris flow to refer to the flow with $C_v=0.5$ and 0.3, respectively. The total volume of a debris flow surge, along with the mass of water and sediment, is detailed in Fig. 2.

In addition, the Froude number ($Fr$) of the debris flows was considered because debris flows are gravitational processes with

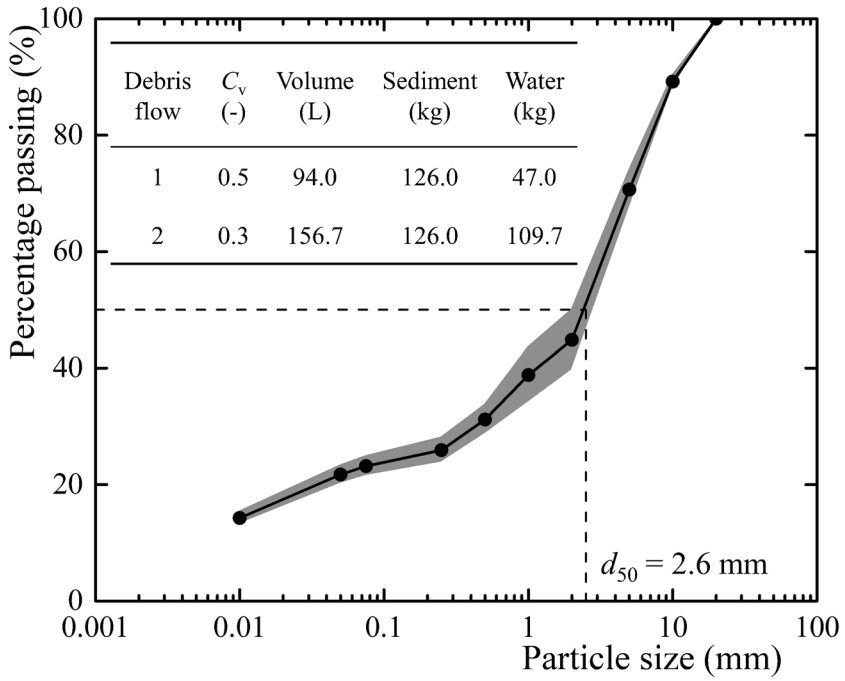


**Fig. 2** Composition of debris flow

open channel flow characteristics (Pudasaini and Kröner 2008; Iverson 2015) and are considered to be closely related to deposition, impact force, and runup height (Choi et al. 2015a; Ng et al. 2019; Zhou et al. 2019b). The *Fr* values were measured at approximately 1 m upstream of the model woods (Fig. 1 and Appendix). The peak *Fr* values were 4.7 and 4.5 for debris flows with $C_v = 0.5$ and 0.3 (Fig. 3), respectively, which are consistent with the *Fr* values of multiple field cases (Choi et al. 2015b; Wang et al. 2022; Du et al. 2023). The maximum flow depths upstream of the model woods were 6.8 ± 0.7 cm and 9.4 ± 1.4 cm for debris flows with $C_v = 0.5$ and 0.3 (Fig. 3), respectively.

Pore water pressure plays a crucial role in debris flow movement. However, in small-scale model tests, debris flows can easily degrade into flow controlled by viscous forces (Iverson 2015). To better simulate the debris flow process, the following measures were taken: (a) We simulated debris flow with the smaller possible sediment volume concentration, in which the impact of pore water pressure is smaller even in the field prototype. (b) We selected debris flow deposits from Jiangjia Gully which are rich in fine particles as our experimental material since an increase in fine particle content helps slow the diffusion of pore water pressure (Yang et al. 2021a, b). (c) We maximized the flow depth to the extent possible within our capabilities (around 10 cm). These efforts effectively reduce the pore pressure diffusion number (Choi et al. 2024). It is also important to note that the tree trunk models used in this study were made of acrylic, and the scaling

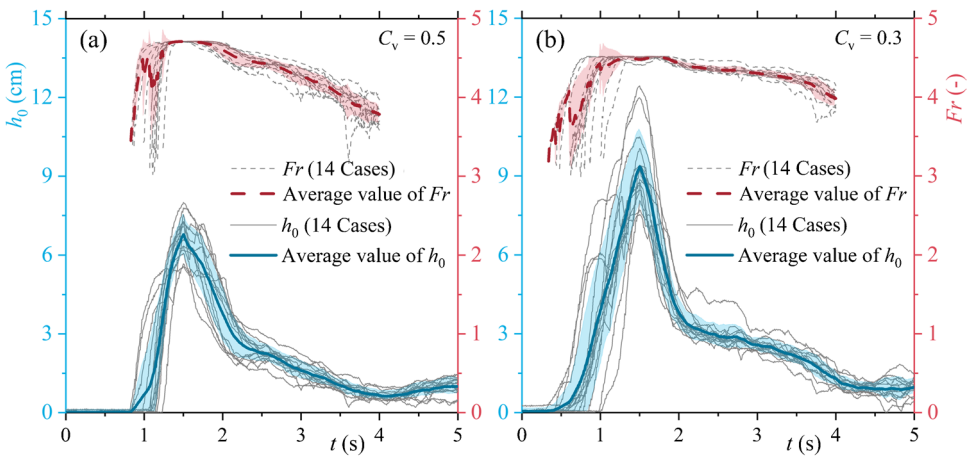


**Fig. 3** The kinematic characteristics of debris flow surges. **a** $C_v = 0.5$; **b** $C_v = 0.3$

effects of the tree trunk material were not strictly considered. Therefore, the impact forces measured in the experiments can only be used to evaluate the impact force attenuation rate ($A_F$) and should be used cautiously for calibrating parameters related to the calculation of debris flow impact forces on tree trunks, such as the dynamic pressure coefficient (Kim et al. 2023).

## Results and analysis

### The regulating mechanism of woods on debris flow

In Fig. 4a, the debris flow process through the wooded channel is illustrated using D1_L8_C0.5 as an example, while Fig. 4b provides a schematic diagram of this process. Figure 4 a-1 displays the initial state of the debris flow head and the wooded channel. In Fig. 4 a-2, the flow characteristics are depicted as the debris flow enters the wooded channel: the debris flow head decelerates upon impact, leading to an increase in flow depth. Additionally, some fluid fragments and leaps forward. As more debris flows enter the wooded area, the flow depth within the wooded channel continues to rise, causing an increase in debris flow depth upstream and near the wooded area, as indicated by the red elevation line in Fig. 4 a-3. Meanwhile, the wooded area, along with the low-velocity fluid within it, collectively obstructs the upstream flow. This obstruction results in an enhanced energy dissipation process, which is evidenced by the increased fragmentation of the fluid, as shown in Fig. 4 a-3. Eventually, the flow velocity, flow depth, and resistance (including both the channel bed and the woods) of the debris flow reach a harmonious equilibrium as they pass through the subsequent woods. After the main part of the debris flow passes through, a backwater pool forms upstream of the wooded channel due to trapped sediment inside the wooded area, as illustrated in Fig. 4 a-4 and b-4.

The passage of debris flow through wooded area can be conceptualized as a complex interplay between the energy slope (Eq. 4) of the debris flow and the slope of the channel bed, as illustrated in Fig. 4c. Initially, prior to entering the woods, the energy slope of the debris flow closely aligned with the slope of the channel bed, indicating a harmonious state. However, upon entering the wooded channel, the resistance offered by the trees caused a rapid increase in the energy slope of the debris flow, creating a mismatch with the channel bed slope. Consequently, the debris flow decelerated, leading to an increase in flow depth and a subsequent decrease in the energy slope, as defined in Eq. 4. Conversely, the slowing down of debris flows facilitated the formation of deposition, as depicted in Fig. 5. The deepest point of deposition was located at the upstream edge of the wooded model and gradually decreased in depth downstream (Fig. 5a). Consequently, the trapped sediment raised the slope of the channel bed within the wooded area. As a result of these combined factors, the energy slope of the debris flow realigned with the slope of the channel bed, leading to the stabilization of the debris flow as it progressed through the subsequent wooded channel, as illustrated in Fig. 4c.

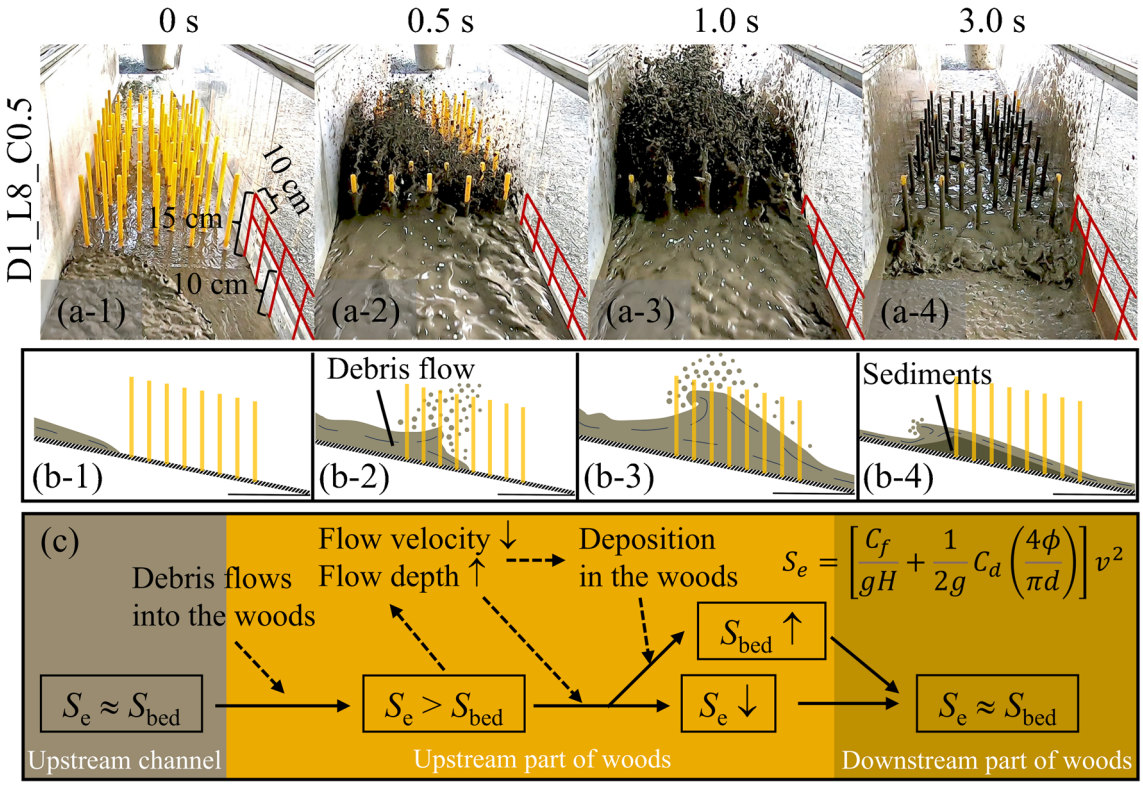


**Fig. 4** The regulation mechanism of woods on debris flow. **a** The process of debris flow through the wooded channel (D1_L8_C0.5). **b** The schematic diagram of this process. **c** The mechanism of this process

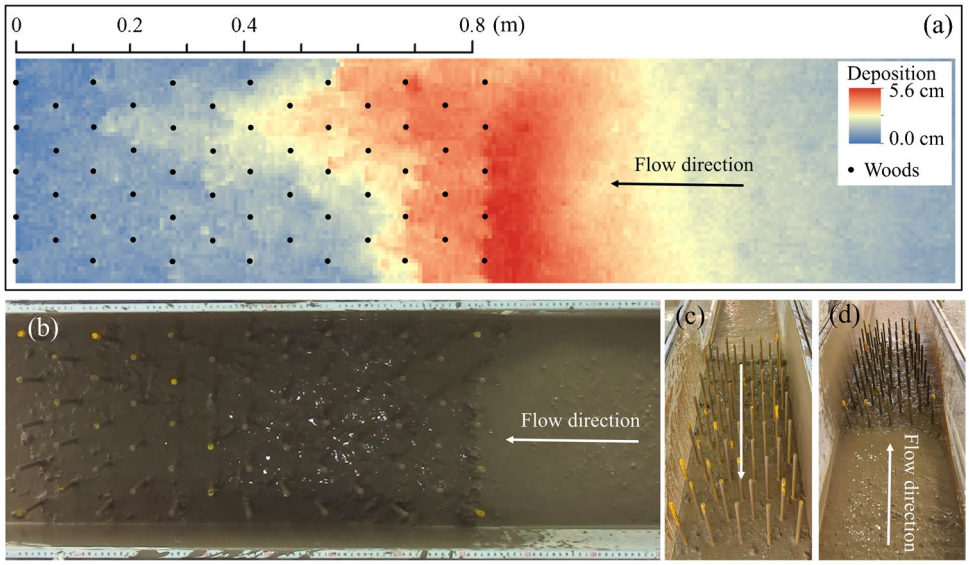


**Fig. 5** The trapped sediment (D1_L8_C0.5). **a** The distribution of trapped sediment. **b** Top view. **c** View from downstream. **d** View from upstream

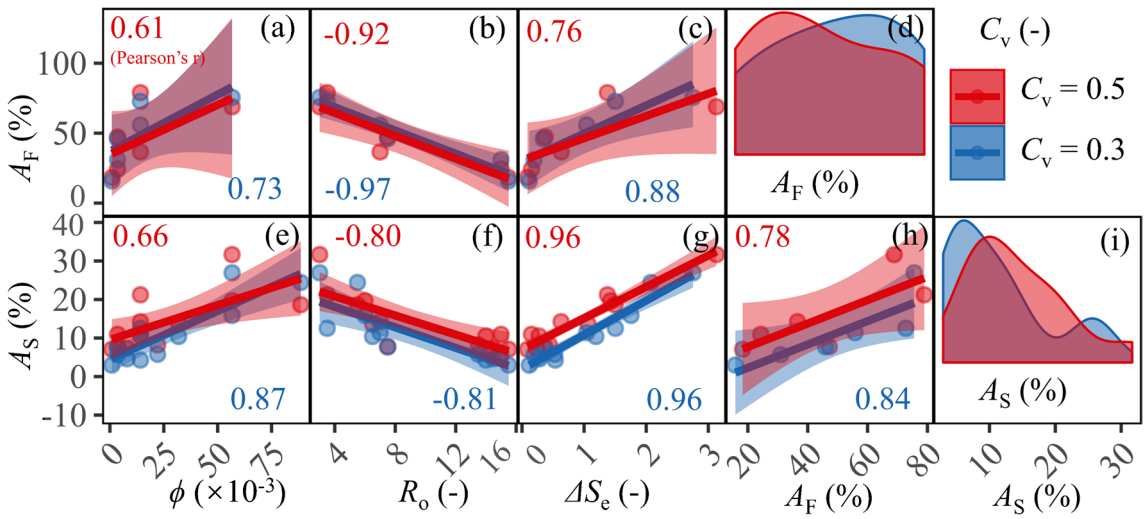


**Fig. 6** The effects of$\phi$, $R_o$, and $\Delta S_e$ on $A_F$ and $A_S$. **a, b, c** The correlation between $A_F$ and ($\phi$, $R_o$, and $\Delta S_e$). **d** The distribution of $A_F$. **e, f, g** The correlation between $A_S$ and ($\phi$, $R_o$, and $\Delta S_e$). **h** The correlation between $A_F$ and $A_S$. **i** The distribution of $A_S$. (Note, $\phi$: the tree trunks volume fraction; $R_o$: the relative opening; $\Delta S_e$: the initial resistance energy slope of woods; $A_F$: the attenuation rate of peak impact force; $A_S$: the sediment retention rate)

### The regulating effect of woods on debris flow dynamics and sediment

The study utilized the attenuation rate of peak impact force ($A_F$) (Eq. 5) and sediment retention rate ($A_S$) (Eq. 7) to gauge the regulatory impact of wooded areas on debris flow dynamics and sediment, respectively. Experimental findings demonstrated a range in $A_F$ from 15.8 to 79.0%. In viscous debris flows, $A_F$ exhibited a mean of 45.7% with a standard deviation of 22.1%, while for diluted debris flows, the mean was 49.5% with a standard deviation of 21.4% (Fig. 6d). Pearson's correlation coefficient ($r$) values were analyzed to assess the relationships of $A_F$ with tree trunks volume fraction ($\phi$), relative opening ($R_o$), and the initial resistance energy slope ($\Delta S_e$), leading to differentiated correlation levels for viscous and diluted debris flows (Table 4). Specifically, for viscous debris flows, $A_F$ showed a highly negative correlation with $R_o$ and a strong positive correlation with $\Delta S_e$ and $\phi$. In contrast, for diluted debris flows, $A_F$ was highly negatively correlated with $R_o$, highly positively correlated with $\Delta S_e$, and strongly positively correlated with $\phi$ (Fig. 6a, b, and c).

**Table 4** The correlation levels based on Pearson's *r*

| \|Pearson's *r*\| | 0.0–0.2 | 0.2–0.4 | 0.4–0.6 | 0.6–0.8 | 0.8–1.0 |
|---|---|---|---|---|---|
| Correlation levels | Negligible | Weak | Moderate | Strong | High |

Additionally, the sediment retention rate ($A_S$) ranged from 3.0 to 31.7%. In viscous debris flows, $A_S$ demonstrated a mean of 14.3% with a standard deviation of 7.1% (Fig. 6i). $A_S$ exhibited a high positive correlation with $\Delta S_e$, a high negative correlation with $R_o$, and a strong positive correlation with $\phi$. For diluted debris flows, the mean $A_S$ was 11.1% with a standard deviation of 7.5%, and it correlated highly with $\Delta S_e$, $\phi$, and $R_o$ (Fig. 6e, f, and g).

Overall, $A_F$ exhibited the strongest correlation with $R_o$ and $A_S$ exhibited the strongest correlation with $\Delta S_e$. Moreover, it was noted that $A_F$ values were slightly smaller in viscous debris flows than in diluted debris flows (Fig. 6d), while $A_S$ values were slightly larger in viscous debris flows than in diluted debris flows (Fig. 6i).

### The volume and distribution of trapped sediment

Figure 7 displays the longitudinal distribution of sediment trapped by the woods model along the channel. The shaded section of the figure represents the wooded channel. In the case of viscous debris flows (Fig. 7a), the maximum deposition height was primarily concentrated upstream of the wooded channel. Notably, the biggest sediment trapping effect was observed in D1_L8_Co.5 and D2_L8_Co.5, corresponding to the two scenarios with the highest stand density (Table 3). Conversely, for diluted debris flows, the maximum deposition height was predominantly situated in the upstream section of the wooded model. Here, the most significant sediment trapping effect was evident in D2_L8_Co.3 and D5_L16_Co.3, aligning with the two conditions boasting the highest tree trunk volume fraction (Table 3). In summary, the impact of trunk diameter on the deposition of diluted debris flows exceeded that of viscous debris flows.

To precisely quantify the location of maximum deposition height and the degree of deposition dispersion shown in Fig. 7, we calculated the expectation ($E(y)$) and variance ($\sigma(y)$) of the deposition position using Eqs. 9 and 10, respectively.

$$E(y) = \frac{BL_{\text{woods}}}{V_{\text{dep}}} \int_0^2 y \cdot H_{\text{dep}}(y) d(y) \tag{9}$$

$$\sigma(y) = \left( \frac{BL_{\text{woods}}}{V_{\text{dep}}} \int_0^2 (y - E(y))^2 \cdot H_{\text{dep}}(y) d(y) \right)^{0.5} \tag{10}$$

$E(y)$ ranged from 0.78 to 1.21. In the case of viscous debris flows, the mean and standard deviation of $E(y)$ were 1.01 and 0.04, respectively (Fig. 8d). $E(y)$ exhibited a moderate correlation with $\phi$, a weak correlation with $R_o$, and negligible correlation with $\Delta S_e$. Conversely, for diluted debris flows, the mean and standard deviation of $E(y)$ were 0.94 and 0.12, respectively. $E(y)$ displayed strong correlations with $\Delta S_e$, moderate correlations with $R_o$ and $\phi$ (Fig. 8a, b, and c). Moreover, $\sigma(y)$ ranged from 0.36 to 0.60. For viscous debris flows, the mean and standard deviation of $\sigma(y)$ were 0.54 and 0.05, respectively (Fig. 8i). $\sigma(y)$ showed a high correlation with $\Delta S_e$ and $R_o$ and strong correlations with $\phi$. In the case of diluted debris flows, the mean and standard deviation of $\sigma(y)$ were 0.49 and 0.08, respectively. $\sigma(y)$ exhibited high correlations with $\Delta S_e$, $R_o$, and $\phi$ (Fig. 8e, f, and g). Overall, $E(y)$ for viscous debris flows was greater than that for diluted debris flows, and $\sigma(y)$ for viscous debris flows was also larger than that for diluted debris flows.

Figure 9 illustrates the influence of tree trunks volume fraction ($\phi$), relative opening ($R_o$), and the initial resistance energy slope ($\Delta S_e$) on the volume ($V_{\text{dep}}$), the maximum height ($H_{\text{max}}$), and the slope increment ($\Delta S_{\text{bed}}$) of the deposition. $V_{\text{dep}}$ ranged from 2.2 to 23.4 L, $H_{\text{max}}$ from 0.5 to 7.2 cm, and $\Delta S_{\text{bed}}$ from 0.002 to 0.089. In the case of viscous debris flows, $V_{\text{dep}}$ had a mean of 10.5 L with a standard deviation of 5.2 L, $H_{\text{max}}$ had a mean of 2.6 cm with a standard

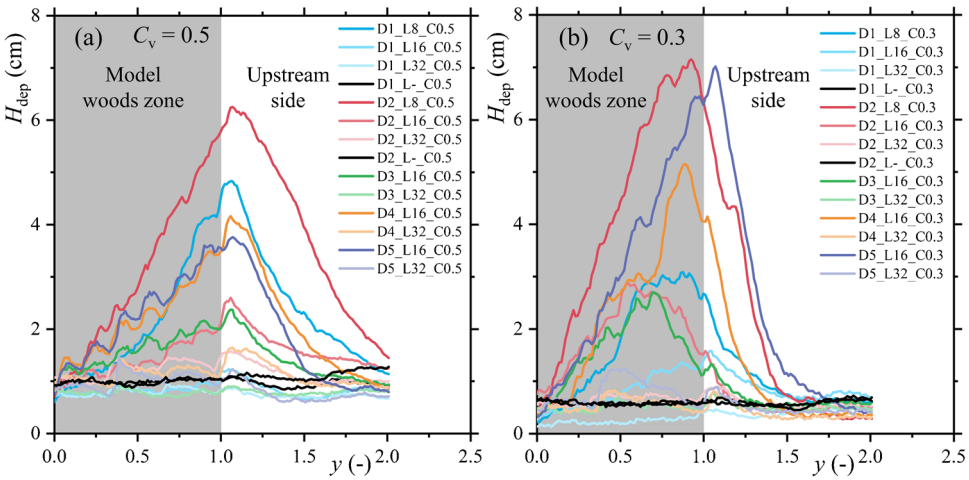


**Fig. 7** The distribution of trapped sediment along channel. **a** $C_v = 0.5$; **b** $C_v = 0.3$

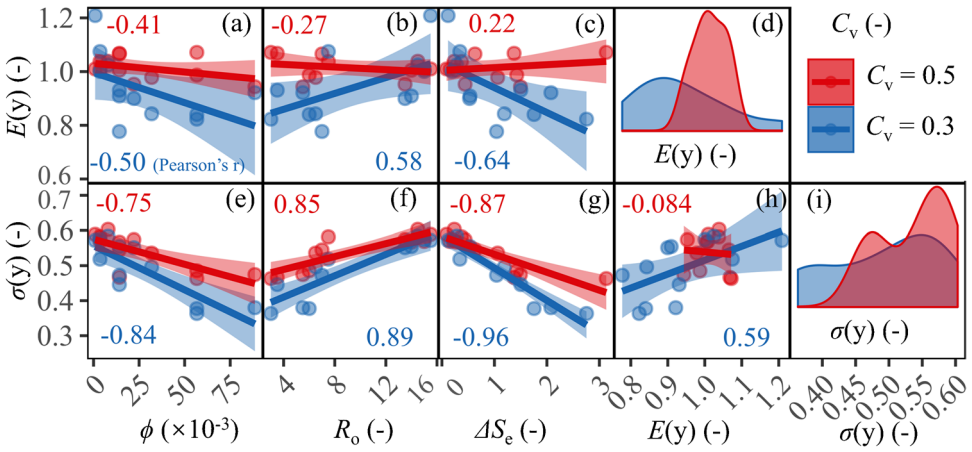


**Fig. 8** The effects of$\phi$, $R_o$, and $\Delta S_e$ on $E(y)$ and $\sigma(y)$. **a, b, c** The correlation between $E(y)$ and ($\phi$, $R_o$, and $\Delta S_e$). **d** The distribution of $E(y)$. **e, f, g** The correlation between $\sigma(y)$ and ($\phi$, $R_o$, and $\Delta S_e$). **h** The correlation between $E(y)$ and $\sigma(y)$. **i** The distribution of $\sigma(y)$. (Note, $\phi$: the tree trunks volume fraction; $R_o$: the relative opening; $\Delta S_e$: the initial resistance energy slope of woods; $E(y)$ and ($\sigma(y)$): the expectation and variance of the deposition position)

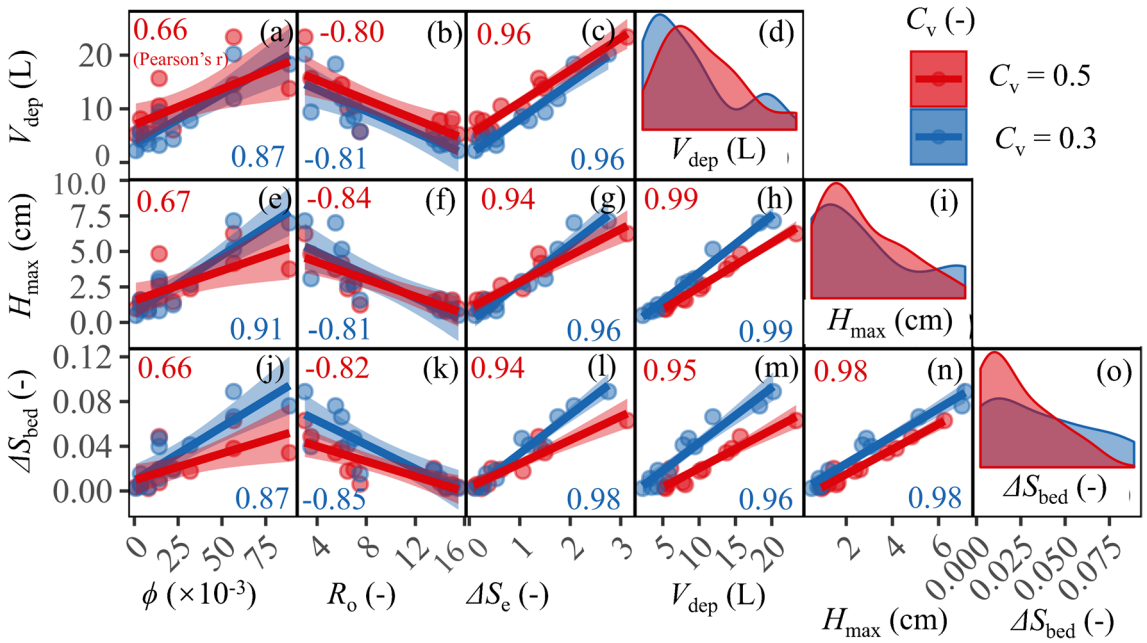


**Fig. 9** The effects of$\phi$, $R_o$, and $\Delta S_e$ on $V_{dep}$, $H_{max}$, and $\Delta S_{bed}$. **a, b, c** The correlation between $V_{dep}$ and ($\phi$, $R_o$, and $\Delta S_e$). **d** The distribution of $V_{dep}$. **e, f, g** The correlation between $H_{max}$ and ($\phi$, $R_o$, and $\Delta S_e$), **h, m, n** The correlation between $V_{dep}$, $H_{max}$, and $\Delta S_{bed}$. **i** The distribution of $H_{max}$. **j, h, l** The correlation between $\Delta S_{bed}$ and ($\phi$, $R_o$, and $\Delta S_e$). **o** The distribution of $\Delta S_{bed}$. (Note, $\phi$: the tree trunks volume fraction; $R_o$: the relative opening; $\Delta S_e$: the initial resistance energy slope of woods; $V_{dep}$, $H_{max}$, and $\Delta S_{bed}$: the volume, maximum height, and slope increment of the deposition)

deviation of 1.65 cm, and $\Delta S_{bed}$ had a mean of 0.022 with a standard deviation of 0.019. Conversely, for diluted debris flows, $V_{dep}$ averaged 8.3 L with a standard deviation of 5.6 L, $H_{max}$ averaged 2.8 cm with a standard deviation of 2.3 cm, and $\Delta S_{bed}$ averaged 0.034 with a standard deviation of 0.029 (Fig. 9d, i, and o).

Additionally, for viscous debris flows, $V_{dep}$, $H_{max}$, and $\Delta S_{bed}$ exhibited high correlations with $\Delta S_e$ and $R_o$, and a strong positive correlation with $\phi$. In contrast, for diluted debris flows, $V_{dep}$, $H_{max}$, and $\Delta S_{bed}$ displayed high correlations with $\Delta S_e$, $R_o$, and $\phi$ (Fig. 9a, b, c, e, f, g, j, k, and l). Overall, $V_{dep}$ for viscous debris flows exceeded that of diluted debris flows, while $H_{max}$ and $\Delta S_{bed}$ for viscous debris flows were smaller compared to those of diluted debris flows. This disparity could be attributed to differences in deposition distribution, as depicted in Fig. 7.

The bed slope increment ($\Delta S_{bed}$) caused by deposition in wooded channel, a dimensionless parameter, exhibited a highly linear correlation between $V_{dep}$ and $H_{max}$, as evident in Fig. 9m and n. Hence, $\Delta S_{bed}$ proved to be of significant research and application

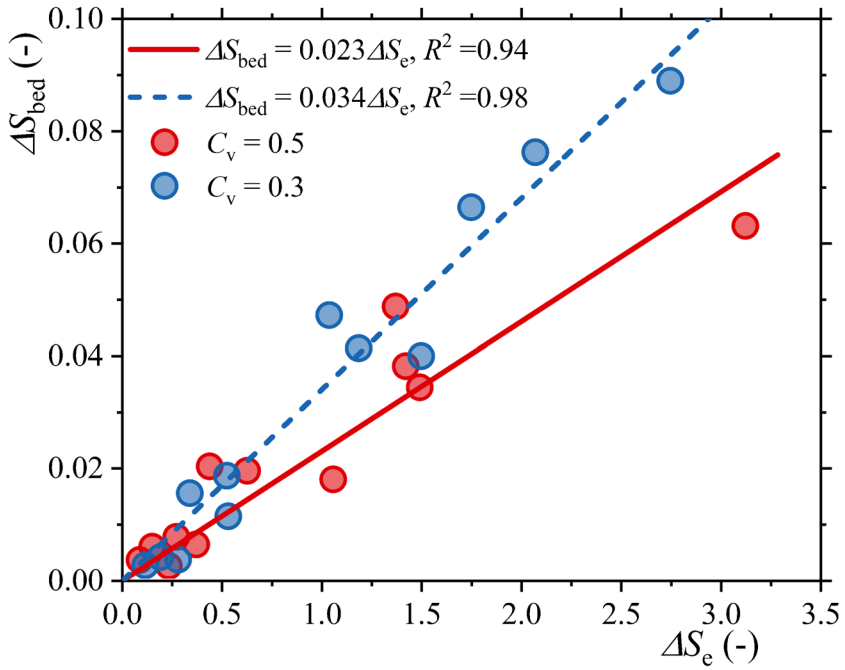


**Fig. 10** The proportional relationship between the wooded channel bed deposition slope increment ($\Delta S_{bed}$) and the initial resistance energy slope of woods ($\Delta S_e$)

value. Notably, $\Delta S_{bed}$ was directly proportional to $\Delta S_e$, as illustrated in Fig. 10, and both parameters shared similar physical interpretations, signifying slope. Their ratios could effectively characterize the conversion efficiency of initial resistance energy slope of woods to deposition slope. Figure 10 demonstrates that $\Delta S_{bed}$ accounts for approximately 2.3% and 3.4% of $\Delta S_e$ for viscous and diluted debris flows, respectively.

## Discussion

### The $\phi$ of natural woods and its regulation capacity on debris flow

This paper investigates the role of channel woods in regulating debris flow movement and sediment retention through physical model experiments. The results reveal that increasing both stand density and breast diameter of trees effectively reduces the peak impact force of debris flow while enhancing sediment trapping capacity. However, it is important to note that natural woods undergo a natural thinning process, meaning that as trees grow and their breast diameter increases, stand density gradually decreases (Reineke 1933; Pretzsch and Biber 2005). Drawing from field data across China (Wu et al. 2023), Europe (Põldveer et al. 2020), and Japan (Ishihara et al. 2011) indicate that the maximum value of $\phi$ in natural forests hovers around $14 \times 10^{-3}$ (Fig. 11).

For conditions where $\phi < 14 \times 10^{-3}$, the maximum values of $A_F$ and $A_S$ were approximately 61.0% and 14.8%, respectively, with a maximum $\Delta S_{bed}$ of about 0.039. This suggests that natural forests within channels possess inherent capabilities to regulate debris flow (Ishikawa et al. 2003; Malik et al. 2013; Michelini et al. 2017). When $\phi$ values are intentionally increased through measures such as adding pile arrays in forests (Ng et al. 2014; Wang et al. 2020), the regulatory capacity of forests to control debris flows is further enhanced (Fig. 11). However, when the number of rows of trees or baffle arrays is too small, their regulatory effects on debris flows will be significantly reduced (Fig. 11, Kim et al. 2023). It is also important to exercise caution in projects where both trees and artificial piles coexist, as excessive local deposition thickness may lead to tree mortality (Ishikawa et al. 2003; Michelini et al. 2017).

### Deposition slope in wooded channel

The deposition slope stands as a pivotal factor in characterizing the landform resulting from debris flow channels (Chen et al. 2016; Piton and Recking 2016). Additionally, it finds widespread application in determining the storage capacity of engineering mitigation projects such as check dams (Huang et al. 2021). Establishing a clear connection between the deposition slope and the parameters of channel woods holds significant implications for the effective utilization of nature-based solutions in debris flow channels (Cui and Lin 2013; Rey and Burylo 2014; Rey et al. 2019). Notably, $\Delta S_{bed}$ demonstrated a direct proportionality to $\Delta S_e$, as demonstrated in Fig. 9. This relationship underscores the crucial interplay between these variables in the context of debris flow regulation:

$$\Delta S_{bed} = k\Delta S_e \tag{11}$$

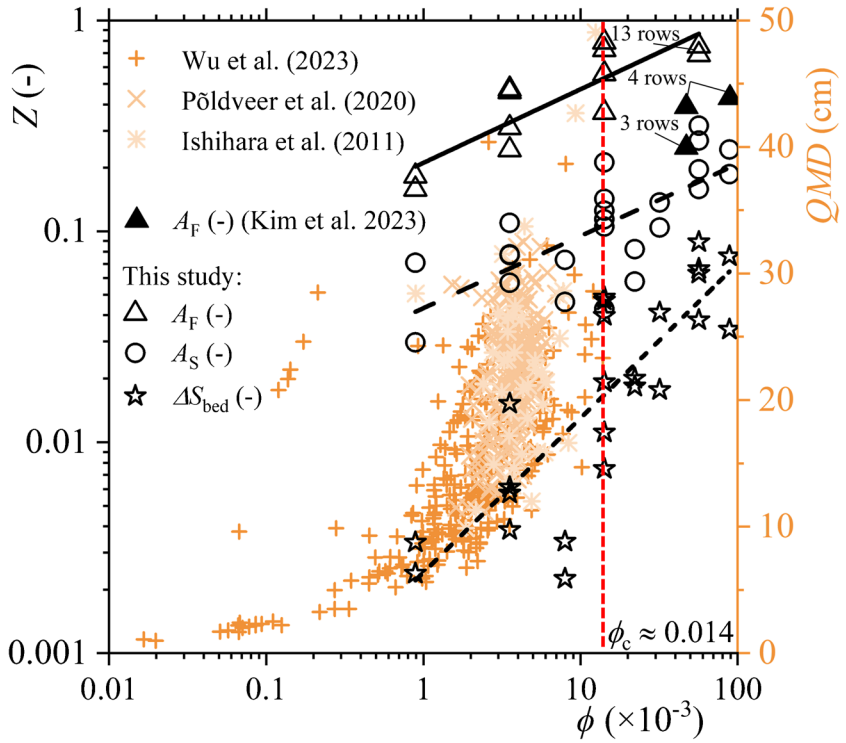


**Fig. 11** The tree trunks volume fraction ($\phi$) of natural woods and its regulation capacity on debris flow. (Note, *Z*: regulation function indexes, such as the attenuation rate of peak impact force ($A_F$), the sediment retention rate ($A_S$), and deposition slope increment ($\Delta S_{dep}$); QMD: quadratic mean diameter of woods. The yellow dots show the relationship between $\phi$ and QMD in natural forests. The black dots represent the variation of *Z* with $\phi$.)

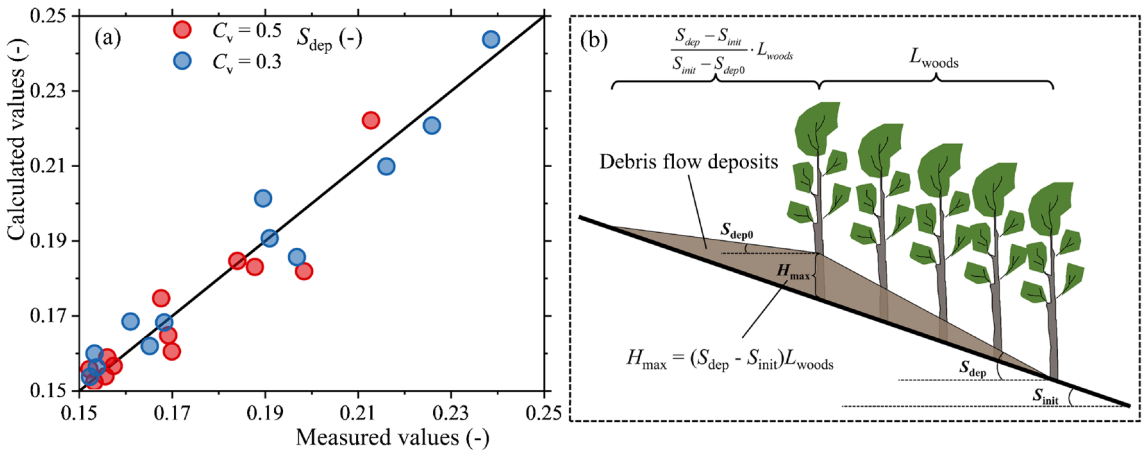


**Fig. 12** **a** Comparison of the calculated and measured values of deposition slope ($S_{dep}$) in a wooded channel. **b** A schematic longitudinal profile of debris flow deposits influenced by channel forests

where *k* is proportional coefficient. By integrating Eqs. 3, 7, and 11, we derive the formula for the deposition slope in a wooded channel ($S_{dep}$).

$$S_{dep} = S_{init} + \frac{k}{2g} C_d \left(\frac{4\phi}{\pi d}\right) v_0^2 \quad (12)$$

where $S_{init}$ is 15% in the study; *k* is approximately 2.3% and 3.4% for viscous debris flows and diluted debris flows, respectively. We assumed $C_d = 1$ in the study (Ishikawa et al. 2003); *g* is 9.8 m/s² in the study. The value of *d* and $\phi$ is shown in Table 3; $\pi$ is approximately 3.14; $v_0$ is shown in a dataset (Wang et al. 2024).

As illustrated in Fig. 12a, Eq. 12 effectively calculates the deposition slope, validating the rationality of its structure. Notably, the parameter $k$ holds significant importance, remaining largely unaffected by tree stand density and breast diameter. It is predominantly influenced by debris flow characteristics, such as density. It is also crucial to note that due to the absence of relevant observational studies, Eq. 12 has not been validated with field data. Therefore, verifying the applicability of Eq. 12 in real-world scenarios and determining the calculation method for $k$ should be addressed in future research efforts.

The deposition slope ($S_{dep}$) in the wooded channel is useful for assessing the potential sediment trapping capacity of channel forests. In a simplified rectangular cross-section channel (Fig. 12b), the potential sediment retained volume ($V_{dep,pot}$) by channel forests can be approximately evaluated using the following equation:

$$V_{dep,\,pot} = \frac{1}{2} \cdot \frac{\left(S_{dep} - S_{init}\right)\left(S_{dep} - S_{dep0}\right)}{S_{init} - S_{dep0}} \cdot L_{woods}^{2} \cdot B \tag{13}$$

where $L_{woods}$ represents the length of the channel forests, $B$ denotes the width of the channel, and $S_{depo}$ is the deposition slope of the debris flow upstream of the forests. The value of $S_{depo}$ can be referenced from studies on the deposition slope upstream of check dams (Chen et al. 2016; Piton and Recking 2016). It is important to note that Eq. 13 assumes the maximum deposition height occurs at the upper edge of the forests. In reality, the maximum deposition depth does not always occur at the upper edge of the forests (Fig. 7). Therefore, Eq. 13 may require appropriate adjustments for practical application.

This study primarily focuses on (1) the macroscopic regulation mechanisms of debris flow by channel forests as a whole (Fig. 4c), and (2) the statistical relationships between the macroscopic characteristics of channel forests and debris flow regulation indices. Future research should enhance the exploration of specific physical processes occurring within channel forests, such as the development and interaction of bow shock waves (Cui et al. 2023b; Liang et al. 2023), and the evolutionary characteristics of flow and impact forces along the channel (Choi et al. 2015c; Ng et al. 2015; Kim et al. 2023). Moreover, in the experiments, efforts were made to control the composition and movement processes of debris flows to minimize the impact of inherent differences in debris flows on the experimental results. Therefore, the influence of the intrinsic characteristics of debris flows on the regulation effects has not been fully considered. The intrinsic characteristics of debris flows (e.g., sediment particle size) significantly impact jamming and deposition (Piton and Recking 2016; Zhou et al. 2019b; Gong et al. 2023), as well as impact forces (Ng et al. 2021). Designing dedicated experiments to quantify and analyze the influence of the intrinsic characteristics of debris flow is also crucial for future research. In constructing the forest model, it is important to enhance the similarity between the model materials and the prototype trees while also considering the randomness of tree distribution and diameter at breast height, as well as the location of the trees. The trees in the upstream, midstream, and downstream sections of the channel may differ significantly in their regulatory effects on debris flows (Cuomo et al. 2017; Cuomo 2020; Sun et al. 2024).

## Conclusions

The regulation effects of channel woods on debris flow movement and deposition were examined through physical model experiments. Based on the obtained results, the following conclusions can be drawn.

(1) Upon entry into channel woods, debris flow experienced a reduction in velocity and an increase in depth, eventually adapting to the new resistance environment and a substantial volume of sediment was trapped in the wooded channel. Deposition depth decreased progressively from upstream to downstream in wooded channels, thereby elevating the slope of the wooded channel bed.

(2) Both the attenuation rate of peak impact force in the downstream end of woods ($A_F$) and the sediment retention rate ($A_S$) exhibited negative correlations with the relative opening ($R_o$), positive correlations with the initial resistance energy slope of woods ($\Delta S_e$) and tree trunk volume fraction ($\phi$). Specifically, $A_F$ demonstrated the strongest correlation with $R_o$, whereas $A_S$ was most strongly correlated with $\Delta S_e$. Viscous debris flows exhibited slightly lower $A_F$ than diluted debris flows, with the reverse being true for $A_S$. In the experiments, the $A_F$ ranged from 15.8 to 79.0%, while the $A_S$ fell between 3.0 and 31.7%.

(3) The bed slope increment($\Delta S_{bed}$) caused by deposition in wooded channel showed negative correlations with $R_o$ and positive correlations with $\Delta S_e$ and $\phi$, with the strongest correlation observed with $\Delta S_e$. $\Delta S_{bed}$ was directly proportional to $\Delta S_e$, accounting for approximately 2.3% and 3.4% of $\Delta S_e$ for viscous and diluted debris flows, respectively. Additionally, a novel method for calculating deposition slope and potential sediment retained volume in wooded channels was introduced.


## Acknowledgements

Support from the Dongchuan Debris Flow Observation and Research Station (DDFORS), Chinese Academy of Sciences, is acknowledged. The authors would also like to thank the journal editors and four anonymous reviewers for their valuable suggestions.

## Funding

This study was supported by the National Natural Science Foundation of China (grant no. 41925030), the Strategic Priority Research Program of the Chinese Academy of Sciences (grant no. XDA23090403), and the Chinese Academy of Sciences Light of West China Program.


## Data availability

The study data could be accessed at https://zenodo.org/records/12539196.

## Declarations

**Competing interests** The authors declare no competing interests.

## Appendix

We cited the previous researches and the calculation method of Froude number (*Fr*) (Domnik and Pudasaini 2012; Choi et al. 2015b; Ng et al. 2019):

$$Fr = \frac{v_0}{\sqrt{gh_0\cos\theta}} \tag{14}$$

where $h_0$ is the flow depth of the debris flow (m) with detailed monitoring methods provided in "Experimental arrangement and measured variables"; $v_0$ is the flow velocity of the debris flow (m/s), and its assessment method described below; $g$ is the gravitational acceleration, $g = 9.8$ m/s$^2$; $\theta$ is the slope angle of channel flume (°), $\theta = 8.5°$.

The improved Manning formula is used to calculate the velocity of debris flow surges (Rickenmann 1999; Hu et al. 2013; Tian et al. 2014). We assume that the debris flow in the flume approximately adheres to Manning's equation, thereby providing a straightforward method for assessing flow velocity.

According to the Manning formula:

$$v_0 = \frac{1}{n}R^{2/3}S_{bed}^{1/2} \tag{15}$$

where $n$ is Manning's roughness coefficient; $R$ is the hydraulic radius (m); $S_{bed}$ is the slope of flume bed (-), $S_{bed} = 0.15$ in this study.

The parameter $R$ can be calculated:

$$R = \frac{A_0}{L_0} = \frac{b_0h_0}{b_0 + 2h_0} \tag{16}$$

where $A_0$ is the cross-sectional area of flow (m$^2$); $L_0$ is the wetted perimeter (m); $b_0$ is the width of channel bed.

The parameter Manning's roughness coefficient ($n$) can be evaluated through the following methods.

The volume ($V_d$) and discharge ($Q_d$) of a debris-flow surge have the following relationship:

$$\int Q_d dt = V_d \tag{17}$$

$$Q_d = v_0A_0 = \frac{1}{n}\left(\frac{b_0h_0}{b_0 + 2h_0}\right)^{2/3} \cdot S_{bed}^{1/2} \cdot b_0h_0 \tag{18}$$

According to Equations 17 and 18, we can obtain following equation:

$$\int Q_d dt \approx \sum\left(\frac{1}{n}\left(\frac{b_0h_0}{b_0 + 2h_0}\right)^{2/3} \cdot S_{bed}^{1/2} \cdot b_0h_0\right)\Delta t = V_d \tag{19}$$

Because the sampling frequency of $h_0$ was 100 Hz, $\Delta t = 0.01$ s. For debris flow with $C_v = 0.5$, when $n = 0.0138$ is taken, $V_d = 94.0 \pm 12.9$ L, a value in close proximity to the true $V_d$ of 94.0 L. For debris flow with $C_v = 0.3$, when $n = 0.0144$ is taken, $V_d = 156.9 \pm 23.2$ L, a value in close proximity to the true $V_d$ of 156.7 L. Therefore, Manning's roughness coefficient is approximately 0.0138 and 0.0144 for debris flow with $C_v = 0.5$ and 0.3, respectively. By substituting Manning's roughness coefficient into Equation 15, the flow velocity can be evaluated. Subsequently, the Froude number can be assessed using Equation 14.

## References


Bathurst JC, Bovolo CI, Cisneros F (2010) Modelling the effect of forest cover on shallow landslides at the river basin scale. Ecol Eng 36(3):317–327. https://doi.org/10.1016/j.ecoleng.2009.05.001

Bettella F, Michelini T, D'Agostino V, Bischetti GB (2018) The ability of tree stems to intercept debris flows in forested fan areas: a laboratory modelling study. J Agric Eng 49(1):42–51. https://doi.org/10.4081/jae.2018.712

Bi H, Fox JC, Li Y, Lei Y, Pang Y (2012) Evaluation of nonlinear equations for predicting diameter from tree height. Can J Forest Res 42(4):789–806. https://doi.org/10.1139/x2012-019

Borga M, Stoffel M, Marchi L, Marra F, Jakob M (2014) Hydrogeomorphic response to extreme rainfall in headwater systems: flash floods and debris flows. J Hydrol 518:194–205. https://doi.org/10.1016/j.jhydrol.2014.05.022

Brasington J, Vericat D, Rychkov I (2012) Modeling river bed morphology, roughness, and surface sedimentology using high resolution terrestrial laser scanning. Water Resour Res 48(11). https://doi.org/10.1029/2012WR012223

Chen XQ, Cui P, You Y, Chen JG, Li D (2015) Engineering measures for debris flow hazard mitigation in the Wenchuan earthquake area. Eng Geol 194:73–85. https://doi.org/10.1016/j.enggeo.2014.10.002

Chen JG, Chen XQ, Zhao WY, You Y (2016) Discussion of "Design of sediment traps with open check dams. I: hydraulic and deposition processes" by Guillaume Piton and Alain Recking. J Hydraul Eng 142(10):07016008. https://doi.org/10.1061/(ASCE)HY.1943-7900.0001160

Choi CE, Ng CWW, Song D, Kwan JHS, Shiu HYK, Ho KKS, Koo RC (2014) Flume investigation of landslide debris–resisting baffles. Can Geotech J 51(5):540–553. https://doi.org/10.1139/cgj-2013-0115

Choi CE, Au-Yeung SCH, Ng CWW, Song D (2015a) Flume investigation of landslide granular debris and water runup mechanisms. Geotech Lett 5(1):28–32. https://doi.org/10.1680/geolett.14.00080

Choi CE, Ng CWW, Au-Yeung SCH, Goodwin SR (2015b) Froude characteristics of both dense granular and water flows in flume modelling. Landslides 12:1197–1206. https://doi.org/10.1007/s10346-015-0628-8

Choi CE, Ng CWW, Law RP, Song D, Kwan JSH, Ho KKS (2015c) Computational investigation of baffle configuration on impedance of channelized debris flow. Can Geotech J 52(2):182–197. https://doi.org/10.1139/cgj-2013-0157

Choi CE, Liang Z (2024) Segmentation and deep learning to digitalize the kinematics of flow-type landslides. Acta Geotech 1–20. https://doi.org/10.1007/s11440-023-02216-5

Choi CE, Ng CWW, Liu H (2024) Flume modeling of debris flows. In: Advances in Debris-flow Science and Practice. Springer International Publishing, pp 93–125

Church M, Jakob M (2020) What is a debris flood? Water Resour Res 56(8):e2020WR027144. https://doi.org/10.1029/2020wr027144

Cui P, Lin Y (2013) Debris-flow treatment: the integration of botanical and geotechnical methods. J Resour Ecol 4(2):97–104. https://doi.org/10.5814/j.issn.1674-764x.2013.02.001

Cui P, Zeng C, Lei Y (2015) Experimental analysis on the impact force of viscous debris flow. Earth Surf Proc Land 40(12):1644–1655. https://doi.org/10.1002/esp.3744

Cui WR, Chen JG, Chen XQ, Tang JB, Jin K (2023a) Debris flow characteristics of the compound channels with vegetated floodplains. Sci Total Environ 868:161586. https://doi.org/10.1016/j.scitotenv.2023.161586

Cui WR, Chen JG, Chen XQ, Song DR, Zhao WY, Jin K (2024) Effect of topographic slope on the interaction between debris flows and riparian forests. Landslides 21(4):889–900. https://doi.org/10.1007/s10346-023-02183-8

Cui WR, Chen JG, Zhao WY, Chen XQ (2023b) Characteristics of wake morphology during debris flow when passing a cylindrical obstacle. Phys Fluids 35(11). https://doi.org/10.1063/5.0171674

Cuomo S (2020) Modelling of flowslides and debris avalanches in natural and engineered slopes: a review. Geoenvironmental Dis 7:1–25. https://doi.org/10.1186/s40677-019-0133-9

Cuomo S, Cascini L, Pastor M, Petrosino S (2017) Modelling the propagation of debris avalanches in presence of obstacles. In Advancing Culture of Living with Landslides: Advances in Landslide Technology Volume 3 (pp. 469–475). Springer International Publishing. https://doi.org/10.1007/978-3-319-53487-9_55

Domnik B, Pudasaini SP (2012) Full two-dimensional rapid chute flows of simple viscoplastic granular materials with a pressure-dependent dynamic slip-velocity and their numerical simulations. J Non-Newton Fluid 173:72–86. https://doi.org/10.1016/j.jnnfm.2012.03.001
Du JH, Zhou GG, Tang H, Turowski J, Cui KF (2023) Classification of stream, hyperconcentrated, and debris flow using dimensional analysis and machine learning. Water Resour Res 59(2). https://doi.org/10.1029/2022wr033242
Enos P (1977) Flow regimes in debris flow. Sedimentology 24(1):133–142. https://doi.org/10.1111/j.1365-3091.1977.tb00123.x
Gong XL, Chen XQ, Chen JG, Song DR (2023) Effects of material composition on deposition characteristics of runoff-generated debris flows. Landslides 20(12):2603–2618. https://doi.org/10.1007/s10346-023-02129-0
Goodwin SR, Choi CE (2020) Slit structures: fundamental mechanisms of mechanical trapping of granular flows. Comput Geotech 119:103376. https://doi.org/10.1016/j.compgeo.2019.103376
Goodwin SR, Choi CE (2021) Translational inertial effects and scaling considerations for coarse granular flows impacting landslide-resisting barriers. J Geotech Geoenviron 147(12):04021153. https://doi.org/10.1061/(asce)gt.1943-5606.0002661
Goodwin SR, Choi CE, Yune CY (2021) Towards rational use of baffle arrays on sloped and horizontal terrain for filtering boulders. Can Geotech J 58(10):1571–1589. https://doi.org/10.1139/cgj-2020-0363
Guo X, Li Y, Cui P, Yan H, Zhuang J (2020) Intermittent viscous debris flow formation in Jiangjia Gully from the perspectives of hydrological processes and material supply. J Hydrol 589:125184. https://doi.org/10.1016/j.jhydrol.2020.125184
He S, Wang D, Fang Y, Lan H (2017) Guidelines for integrating ecological and biological engineering technologies for control of severe erosion in mountainous areas–a case study of the Xiaojiang River Basin. China Int Soil Water Conse 5(4):335–344. https://doi.org/10.1016/j.iswcr.2017.05.001
Hu K, Tian M, Li Y (2013) Influence of flow width on mean velocity of debris flows in wide open channel. J Hydraul Eng 139(1):65–69. https://doi.org/10.1061/(ASCE)HY.1943-7900.0000648
Huang T, Ding M, Gao Z, Téllez RD (2021) Check dam storage capacity calculation based on high-resolution topogrammetry: case study of the Cutou Gully, Wenchuan County, China. Sci Total Environ 148083. https://doi.org/10.1016/j.scitotenv.2021.148083
Huebl J, Kaitna R (2021) Monitoring debris-flow surges and triggering rainfall at the Lattenbach Creek. Austria Environ Eng Geosci 27(2):213–220. https://doi.org/10.2113/EEG-D-20-00010
Imaizumi F, Sidle RC, Kamei R (2008) Effects of forest harvesting on the occurrence of landslides and debris flows in steep terrain of central Japan. Earth Surf Process Landf 33(6):827–840. https://doi.org/10.1002/esp.1574
Ishihara MI, Suzuki SN, Nakamura M, Enoki T, Fujiwara A, Hiura T, Yoshida Y (2011) Forest stand structure, composition, and dynamics in 34 sites over Japan. Ecol Res 26(6):1007. https://doi.org/10.1016/s0378-1127(02)00018-x
Ishikawa Y, Kawakami S, Morimoto C, Mizuhara K (2003) Suppression of debris movement by forests and damage to forests by debris deposition. J Forestry Res 8(1):0037–0047. https://doi.org/10.1007/s103100300004
Iverson RM (1997) The physics of debris flows. Rev Geophys 35(3):245–296. https://doi.org/10.1029/97RG00426
Iverson RM (2015) Scaling and design of landslide and debris-flow experiments. Geomorphology 244:9–20. https://doi.org/10.1016/j.geomorph.2015.02.033
Jan CD, Shen HW (1997) Review dynamic modeling of debris flows. In: Armanini A, Michiue M (eds) Recent developments on debris flows. Lecture Notes in Earth Sciences, vol 64. Springer, Heidelberg. https://doi.org/10.1007/BFb0117764
Kang ZC, Li ZF, Ma AN, Luo JT (2004) Debris flow research in China. Science Publisher, Beijing, pp 16–22
Kean JW, McCoy SW, Tucker GE, Staley DM, Coe JA (2013) Runoff-generated debris flows: observations and modeling of surge initiation, magnitude, and frequency. J Geophys Res-Earth 118(4):2190–2207. https://doi.org/10.1002/jgrf.20148
Khoshkonesh A, Daliri M, Riaz K, Dehrashid FA, Bahmanpouri F, Di Francesco S (2022) Dam-break flow dynamics over a stepped channel with vegetation. J Hydrol 613:128395. https://doi.org/10.1016/j.jhydrol.2022.128395
Kim D, Im S, Lee C, Woo C (2013) Modeling the contribution of trees to shallow landslide development in a steep, forested watershed. Ecol Eng 61:658–668. https://doi.org/10.1016/j.ecoleng.2013.05.003
Kim BJ, Choi CE, Yune CY (2023) Multi-scale flume investigation of the influence of cylindrical baffles on the mobility of landslide debris. Eng Geol 314:107012. https://doi.org/10.1016/j.enggeo.2023.107012
Kwan JS, Lam C, Choi CE (2024) Advances in design of barriers for debris flow impact. Advances in Debris-flow Science and Practice. Springer International Publishing, Cham, pp 539–563
Li S, You Y, Chen X, Liu J, Chen J (2019) Regulation effectiveness of a window-check dam on debris flows. Eng Geol 253:205–213. https://doi.org/10.1016/j.enggeo.2019.03.020
Li Q, Zeng YH, Zha W (2020) Velocity distribution and turbulence structure of open channel flow with floating-leaved vegetation. J Hydrol 590:125298. https://doi.org/10.1016/j.jhydrol.2020.125298
Liang Z, Choi CE, Zhao Y, Jiang Y, Choo J (2023) Revealing the role of forests in the mobility of geophysical flows. Comput Geotech 155:105194. https://doi.org/10.1016/j.compgeo.2022.105194
Lightbody AF, Kui L, Stella JC, Skorko KW, Bywater-Reyes S, Wilcox AC (2019) Riparian vegetation and sediment supply regulate the morphodynamic response of an experimental stream to floods. Front Environ Sci 7:40. https://doi.org/10.3389/fenvs.2019.00040
Liu C, Shan Y, Nepf H (2021) Impact of stem size on turbulence and sediment resuspension under unidirectional flow. Water Resour Res 57(3):e2020WR028620. https://doi.org/10.1029/2020wr028620
Liu C, Yan C, Sun S, Lei J, Nepf H, Shan Y (2022) Velocity, turbulence, and sediment deposition in a channel partially filled with a phragmites australis canopy. Water Resour Res 58(8):e2022WR032381. https://doi.org/10.1029/2022wr032381
Liu Y, Han J, Liu Y, Zhang S, Min L, Liu B, ... Zhang L (2023) Effects of soil and water conservation measures of slope surfaces on flood peaks of small watersheds: a study based on three extreme rainstorm events in northern China. Catena 232:107432. https://doi.org/10.1016/j.catena.2023.107432
Malik I, Tie Y, Owczarek P, Wistuba M, Pilorz W, Woskowicz-Ślęzak B (2013) Human-planted alder trees as a protection against debris flows (a dendrochronological study from the Moxi Basin, Southwestern China). Geochronometria 40(3):208–216. https://doi.org/10.2478/s13386-013-0113-x
Michelini T, Bettella F, D'Agostino V (2017) Field investigations of the interaction between debris flows and forest vegetation in two Alpine fans. Geomorphology 279:150–164. https://doi.org/10.1016/j.geomorph.2016.09.029
Nepf HM (2012) Flow and transport in regions with aquatic vegetation. Annu Rev Fluid Mech 44:123–142. https://doi.org/10.1146/annurev-fluid-120710-101048
Ng CWW, Choi CE, Kwan JSH, Koo RCH, Shiu HYK, Ho KKS (2014) Effects of baffle transverse blockage on landslide debris impedance. Procedia Earth Planet Sci 9:3–13. https://doi.org/10.1016/j.proeps.2014.06.012
Ng CWW, Choi CE, Song D, Kwan JHS, Koo RCH, Shiu HYK, Ho KKS (2015) Physical modeling of baffles influence on landslide debris mobility. Landslides 12:1–18. https://doi.org/10.1007/s10346-014-0476-y
Ng CWW, Kamchoom V, Leung AK (2016) Centrifuge modelling of the effects of root geometry on transpiration-induced suction and stability of vegetated slopes. Landslides 13(5):925–938. https://doi.org/10.1007/s10346-015-0645-7
Ng CWW, Choi CE, Goodwin SR (2019) Froude characterization for unsteady single-surge dry granular flows: impact pressure and runup height. Can Geotech J 56(12):1968–1978. https://doi.org/10.1139/cgj-2018-0529
Ng CWW, Liu H, Choi CE, Kwan JS, Pun WK (2021) Impact dynamics of boulder-enriched debris flow on a rigid barrier. J Geotech Geoenviron 147(3):04021004. https://doi.org/10.1061/(ASCE)GT.1943-5606.0002485
Phillips CJ, Davies TR (1991) Determining rheological parameters of debris flow material. Geomorphology 4(2):101–110. https://doi.org/10.1016/0169-555X(91)90022-3
Piton G, Recking A (2016) Design of sediment traps with open check dams. I: hydraulic and deposition processes. J Hydraul Eng 142(2):04015045. https://doi.org/10.1061/(asce)hy.1943-7900.0001048
Piton G, Goodwin SR, Mark E, Strouth A (2022) Debris flows, boulders and constrictions: a simple framework for modeling jamming, and its consequences on outflow. J Geophys Res-Earth 127(5):e2021JF006447. https://doi.org/10.1029/2021JF006447
Põldveer E, Korjus H, Kiviste A, Kangur A, Paluots T, Laarmann D (2020) Assessment of spatial stand structure of hemiboreal conifer dominated forests according to different levels of naturalness. Ecol Indic 110:105944. https://doi.org/10.1016/j.ecolind.2019.105944

Pretzsch H, Biber P (2005) A re-evaluation of Reineke's rule and stand density index. For Sci 51(4):304–320. https://doi.org/10.1093/forestscience/51.4.304
Pudasaini SP, Kröner C (2008) Shock waves in rapid flows of dense granular materials: theoretical predictions and experimental results. Phys Rev E Stat Nonlinear Soft Matter Phys 78(4 Pt 1):041308. https://doi.org/10.1103/PhysRevE.78.041308
Pudasaini SP, Mergili M (2019) A multi-phase mass flow model. J Geophys Res Earth Surf 124(12):2920–2942. https://doi.org/10.1029/2019JF005204
Reineke LH (1933) Perfecting a stand-density index for even-aged forests. J Agric Res 46:627–638
Rey F, Burylo M (2014) Can bioengineering structures made of willow cuttings trap sediment in eroded marly gullies in a Mediterranean mountainous climate? Geomorphology 204:564–572. https://doi.org/10.1016/j.geomorph.2013.09.003
Rey F, Bifulco C, Bischetti GB, Bourrier F, De Cesare G, Florineth F, Stokes A (2019) Soil and water bioengineering: practice and research needs for reconciling natural hazard control and ecological restoration. Sci Total Environ 648:1210–1218. https://doi.org/10.1016/j.scitotenv.2018.08.217
Rickenmann D (1999) Empirical relationships for debris flows. Nat Hazards 19(1):47–77. https://doi.org/10.1023/A:1008064220727
Schwarz M, Giadrossich F, Cohen D (2013) Modeling root reinforcement using a root-failure Weibull survival function. Hydrol Earth Syst Sci 17(11):4367–4377. https://doi.org/10.5194/hess-17-4367-2013
Schwarz M, Rist A, Cohen D, Giadrossich F, Egorov P, Büttner D, Thormann JJ (2015) Root reinforcement of soils under compression. J Geophys Res Earth Surf 120(10):2103–2120. https://doi.org/10.1002/2015jf003632
Shan Y, Zhao T, Liu C, Nepf H (2020) Turbulence and bed load transport in channels with randomly distributed emergent patches of model vegetation. Geophys Res Lett 47(12):e2020GL087055. https://doi.org/10.1029/2020gl087055
Shima J, Moriyama H, Kokuryo H, Ishikawa N, Mizuyama T (2016) Prevention and mitigation of debris flow hazards by using steel open-type sabo dams. Int J Eros Control Eng 9(3):135–144. https://doi.org/10.13101/ijece.9.135
Silva M, Costa S, Canelas RB, Pinheiro AN, Cardoso AH (2016) Experimental and numerical study of slit-check dams. Int J Sustain Dev Plann 11(2):107–118. https://doi.org/10.2495/sdp-v11-n2-107-118
Stokes A, Douglas GB, Fourcaud T, Giadrossich F, Gillies C, Hubble T, Walker LR (2014) Ecological mitigation of hillslope instability: ten key issues facing researchers and practitioners. Plant Soil 377:1–23. https://doi.org/10.1007/s11104-014-2044-6
Sun H, You Y, Liu J (2018) Experimental study on blocking and self-cleaning behaviors of beam dam in debris flow hazard mitigation. Int J Sediment Res 33(4):395–405. https://doi.org/10.1016/j.ijsrc.2018.04.004
Sun X, Chen M, Bi Y, Zheng L, Che C, Xu A, Jiang Z (2024) Protective effects of baffles with different positions, row spacings, heights on debris flow impact. J Mt Sci 21(7):2352–2367. https://doi.org/10.1007/s11629-024-8658-0
Tanino Y, Nepf HM (2008) Lateral dispersion in random cylinder arrays at high Reynolds number. J Fluid Mech 600:339–371. https://doi.org/10.1017/s0022112008000505
Tian M, Hu KH, Ma C, Lei FH (2014) Effect of bed sediment entrainment on debris-flow resistance. J Hydraul Eng 140(1):115–120. https://doi.org/10.1061/(ASCE)HY.1943-7900.000080
Tinoco RO, Coco G (2016) A laboratory study on sediment resuspension within arrays of rigid cylinders. Adv Water Resour 92:1–9. https://doi.org/10.1016/j.advwatres.2016.04.003
Trujillo-Vela MG, Ramos-Cañón AM, Escobar-Vargas JA, Galindo-Torres SA (2022) An overview of debris-flow mathematical modelling. Earth Sci Rev 104135. https://doi.org/10.1016/j.earscirev.2022.104135
Vargas-Luna A, Crosato A, Anders N, Hoitink AJ, Keesstra SD, Uijttewaal WS (2018) Morphodynamic effects of riparian vegetation growth after stream restoration. Earth Surf Process Landf 43(8):1591–1607. https://doi.org/10.1002/esp.4338
Wang F, Chen X, Chen J, You Y (2017) Experimental study on a debris-flow drainage channel with different types of energy dissipation baffles. Eng Geol 220:43–51. https://doi.org/10.1016/j.enggeo.2017.01.014
Wang D, Li Q, Bi Y, He S (2020) Effects of new baffles system under the impact of rock avalanches. Eng Geol 264:105261. https://doi.org/10.1016/j.enggeo.2019.105261
Wang XA, Chen JG, Chen HY, Chen XQ, Li S, Zhao WY (2022) Erosion process of multiple debris flow surges caused by check dam removal: an experimental study. Water Resour Res 58(3):e2021WR030688. https://doi.org/10.1029/2021wr030688
Wang X, Gualtieri C, Huai W (2023) Grain shear stress and bed-load transport in open channel flow with emergent vegetation. J Hydrol 618:129204. https://doi.org/10.1016/j.jhydrol.2023.129204
Wang XA, Chen JG, Chen XQ (2024) Deposition characteristics of debris flows in wooded channel. Zenodo. https://doi.org/10.5281/zenodo.12539196
Wu X, Jiang X, Liu H, Allen C, Li X, Wang P, ... Chen D (2023) CPSDv0: a forest stand structure database for plantation forests in China. Big Earth Data 7(1):212–230. https://doi.org/10.1080/20964471.2021.2012911
Yang JQ, Nepf HM (2018) A turbulence-based bed-load transport model for bare and vegetated channels. Geophys Res Lett 45(19):10–428. https://doi.org/10.1029/2018gl079319
Yang JQ, Nepf HM (2019) Impact of vegetation on bed load transport rate and bedform characteristics. Water Resour Res 55(7):6109–6124. https://doi.org/10.1029/2018wr024404
Yang CJ, Jen CH, Cheng YC, Lin JC (2021a) Quantification of mudcracks-driven erosion using terrestrial laser scanning in laboratory runoff experiment. Geomorphology 375:107527. https://doi.org/10.1016/j.geomorph.2020.107527
Yang T, Liu D, Li Y, Guo X, Zhang J, Jiang Y (2021b) Grain configuration effect on pore water pressure in debris flow. Front Earth Sci 9:660634. https://doi.org/10.3389/feart.2021.660634
Zanuttigh B, Lamberti A (2007) Instability and surge development in debris flows. Rev Geophys 45(3). https://doi.org/10.1029/2005rg000175
Zhang B, Huang Y, Liu J (2021) Micro-mechanism and efficiency of baffle structure in deceleration of granular flows. Acta Geotech 16:3667–3688. https://doi.org/10.1007/s11440-021-01290-x
Zhou GG, Hu HS, Song D, Zhao T, Chen XQ (2019a) Experimental study on the regulation function of slit dam against debris flows. Landslides 16:75–90. https://doi.org/10.1007/s10346-018-1065-2
Zhou GG, Li S, Song D, Choi CE, Chen X (2019b) Depositional mechanisms and morphology of debris flow: physical modelling. Landslides 16:315–332. https://doi.org/10.1007/s10346-018-1095-9
Zhou G, Lyu L, Xu M, Ma C, Wang Y, Wang Y, Stoffel M (2023) Assessment of check dams and afforestation in mitigating debris flows based on dendrogeomorphic reconstructions, field surveys and semi-empirical models. Catena 232:107434. https://doi.org/10.1016/j.catena.2023.107434



**Xi'an Wang · Jiangang Chen (✉) · Xiaoqing Chen · Huayong Chen · Wanyu Zhao · Xiangning Li · Wenjing Xu**
State Key Laboratory of Mountain Hazards and Engineering Resilience, Institute of Mountain Hazards and Environment, Chinese Academy of Sciences, Chengdu 610299, China
Email: chenjg@imde.ac.cn

**Xi'an Wang · Jiangang Chen · Xiaoqing Chen · Huayong Chen · Wanyu Zhao · Xiangning Li · Wenjing Xu**
University of Chinese Academy Sciences, Beijing 100049, China

**Jiangang Chen · Xiaoqing Chen · Huayong Chen · Wanyu Zhao**
Sichuan Province Engineering Technology Research Center of Mountain Hazard Mitigation, Chengdu 610299, China